DOI:
10.1063/1.1896356

Document Version
Early version, also known as pre-print

Plasmon resonances on metal tips: Understanding tip-enhanced Raman scattering

A. L. Demming,[a] F. Festy, and D. Richards
Department of Physics, King's College London, Strand, London WC2R 2LS, United Kingdom

(Received 30 November 2004; accepted 1 March 2005; published online 12 May 2005)

Calculations of the electric-field enhancements in the vicinity of an illuminated silver tip, modeled using a Drude dielectric response, have been performed using the finite difference time domain method. Tip-induced field enhancements, of application in "apertureless" Raman scanning near-field optical microscopy (SNOM), result from the resonant excitation of plasmons on the metal tip. The sharpness of the plasmon resonance spectrum and the highly localized nature of these modes impose conditions to better exploit tip plasmons in tip-enhanced apertureless SNOM. The effect of tip-to-substrate separation and polarization on the resolution and enhancement are analyzed, with emphasis on the different field components parallel and perpendicular to the substrate. © *2005 American Institute of Physics*. [DOI: 10.1063/1.1896356]

I. INTRODUCTION

The plethora of applications poignant to Raman spectroscopy and nanolithography have inspired intense investigation into near-field enhancement mechanisms.[1–4] The use of metal tips in "apertureless" scanning near-field optical microscopy (SNOM) offers a convenient and controllable way of increasing the total-to-incident-field ratio through the high curvature at the point of the probe and the excitation of localized surface plasmons.[5–9] High spatial resolutions are associated with the field enhancements from apertureless probes, particularly as they are not limited by the aperture size.[10,11] Thus apertureless SNOM probe field enhancements lend themselves to processes which utilize local fields to modify surface chemistries[12] and to manipulate the position of nanoparticles[13–15] and fluorescent behavior in molecules.[16–19] These probes can also be used to enhance the modest Raman cross section, otherwise limited to around 10^{-30} cm^2, some 14 orders of magnitude lower than fluorescence cross sections. The retrieval of a high signal in the presence of background fields has proven an enduring challenge in recent studies.[20,21] An appreciation of the resonant nature of metal tip systems and the sensitivity of such resonances to system geometry and chemical composition appears vital.[22–29] Although the overall enhancement factor is a major goal in such studies, the alignment of field enhancements with molecular orientation is also pertinent and may affect the conditions for optimum performance.

Although approximations of tip geometry are able to provide useful qualitative information[6,30] to obtain an in-depth understanding of electric-field enhancements in the vicinity of an illuminated metal tip employed in apertureless SNOM, it is essential to perform full three-dimensional calculations of the electromagnetic-field distributions in the vicinity of a realistically modeled tip. In particular, it is necessary to account for both the axial and extended geometry of the tip and the frequency-dependent response of the tip metal. The finite difference time domain (FDTD) method has been applied successfully in the past to problems concerning more realistic tip shapes.[9,31] Here we use FDTD to investigate the effect on resonance wavelength and the enhancement factor in a metal tip and glass substrate system[7] (shown in Fig. 1) as tip geometry and tip-to-substrate separation are altered. We also consider the influence of incident light polarization on the resonant response of the relative magnitudes of enhancements parallel and perpendicular to the substrate plane.

II. THE FDTD MODEL

FDTD is a numerical algorithm which solves a discrete formulation of Maxwell's equations to calculate field values throughout a defined problem space after each of a series of time steps.[32] Charge distributions may be calculated from the divergence of the electric field. For the purpose of defining the material parameters to describe a particular system, the problem space is discretized into theoretical blocks called Yee cells.

The system under investigation here comprises a metal cone with a spherical tip positioned in air above a glass substrate of refractive index 1.5 (see Fig. 1).[7] Silver and gold are attractive metals to consider in the study of field enhancements since they conveniently exhibit resonance peaks in the visible range. Here an approximation to a silver tip over a glass substrate is modeled using a Drude response for the frequency-dependent dielectric properties of the metal, $\hat{\varepsilon}(\omega)$,

$$\hat{\varepsilon}(\omega) = 1 - \frac{\omega_p^2}{\omega(\omega + i\gamma)}, \tag{1}$$

where ω_p is the plasmon frequency and γ is the damping parameter. This Drude form does not account for interband transitions in the frequency-dependent dielectric response of silver; however, by applying appropriate parameters, a match with the experimentally obtained dielectric-response values

[a]Electronic mail: anna.demming@kcl.ac.uk

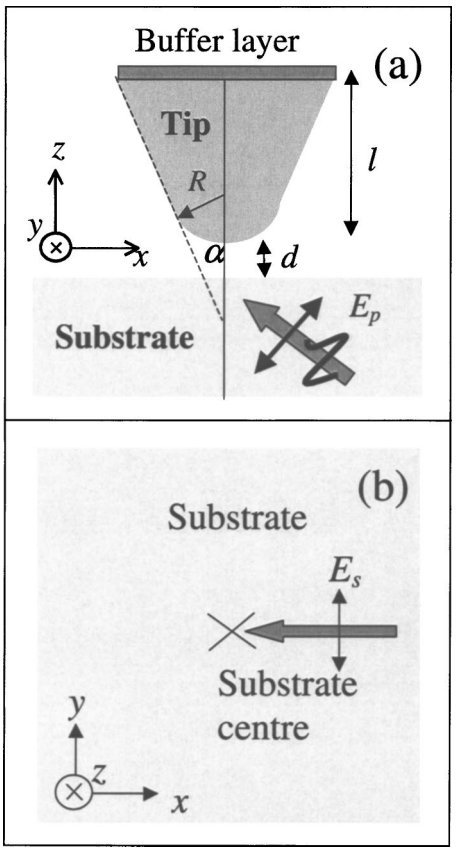

FIG. 1. The configuration of the problem space employed for a metal tip above a glass substrate. (a) The plane of incidence: R indicates the radius of curvature at the end of the tip, d the distance between the base of the tip and the substrate, θ the angle of incidence, and α the cone opening angle. The electric-field vector, E_p, is shown in the instance of p-polarized incident illumination. (b) The substrate plane: the electric-field vector, E_s, is given in the instance of s-polarized incident illumination. The apex of the tip is directly above the substrate center.

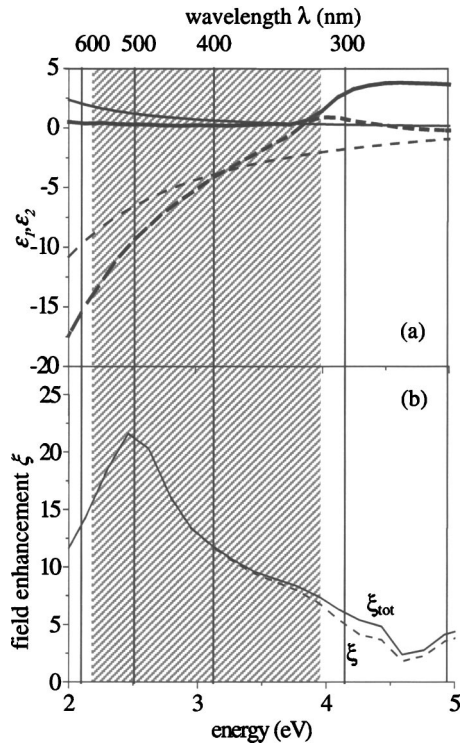

FIG. 2. (a) A comparison of the Drude model (thin lines) for the dielectric response of silver with that of real silver taken from Ref. 32 (bold lines). $\omega_p = 7$ eV and $\gamma = 0.4$ eV for the Drude model. The real (ε_1) and imaginary (ε_2) parts of the dielectric response are indicated by the dashed and solid lines, respectively. The shaded area indicates the range over which the Drude model may be considered to describe real silver. (b) Total, ξ_{tot} (solid) and z component, ξ_z (dashed) field enhancement spectrum on the substrate surface, directly beneath the tip, for p-polarized excitation and $d = 5$ nm. The spectrum exhibits a broad peak at $\lambda = 505$ nm, which is dominated by the z component.

for silver can be achieved over the visible range of the spectrum.[9] Figure 2(a) demonstrates how the Drude model for the dielectric response of silver compares with experimental values.[33] By using a plasmon frequency, ω_p, of 7 eV, and a damping parameter, γ, of 0.4 eV, the fit of the Drude-modeled response and the experimental values from 2.25 to 4 eV (i.e., photon wavelength of $\lambda = 310-550$ nm) is good enough to consider the Drude metal as a model for silver within this range.

Second-order Mur boundary conditions were implemented to inhibit reflections at the extremities of the problem space.[32,34] Mur boundary conditions cannot be applied at the interface of boundary with frequency-dependent materials, such as the metal tip. Thus a buffer layer matched to the dielectric response of the tip material corresponding to typical frequency at which resonances were supported in the system of $\omega = 3$ eV (photon wavelength $\lambda = 414$ m) is introduced between the tip metal and the boundary. Although small changes in the tip length do not affect the resonance of the system, deficiencies in the model's resemblance to an extended tip were revealed when the tip length was varied further in a problem space double the size. This is considered in detail in the final section in order to define the limitations of the current study. Nevertheless, as an approximation, the system investigated is a valid reference point towards the behavior of an apertureless SNOM probe as it interacts with light. Because of the nature of resonant systems, the algorithm was prone to exaggerate numerical errors. In order to hold the propagation of these errors in check, symmetrizing procedures were called within the algorithm.

The FDTD simulations involve the excitation of the tip system with an incident plane-wave pulse. In all of the calculations presented here, the incident pulse was analytically described by a Gaussian derivative. This is important when studying resonant behavior as the system is thus exposed to a continuum of frequencies peaking around the resonant frequency of the system and analysis of the resulting enhancement spectrum allows the resonance to be clearly identified. A frequency-dependent expression for the Drude response of the tip is necessary to avoid instability at resonance and to accommodate an incident pulse covering a range of frequencies. The Drude response is computationally cumbersome once translated into the time domain, however, fortunately the Debye response function behaves more accommodatingly. Consequently, the Drude response is reformulated as a Debye response with specific relations between the parameters.[32]

The pulse was considered incident from beneath a glass substrate at 40° to the normal so that on refraction at the glass-air interface, it propagated near parallel to the substrate

surface. This corresponds to illumination from the perimeter of an objective lens of numerical aperture ~0.95. The *z* axis was defined to run parallel with the tip axis and the *x* and *y* coordinates lie in the plane of the substrate surface such that the refracted *p*-polarized pulse would propagate approximately parallel to the *x* axis with the polarization close to parallel with the tip axis, Fig. 1(a), while *s*-polarized illumination would be polarized parallel with the *y* axis [Fig. 1(b)]. The standard setup, for the purposes of comparison, used a tip comprised of a sphere of radius $R=20$ nm opening at $\alpha=30°$ into a cone, positioned $d=5$ nm above a glass substrate, with *p*-polarized illumination. The radius of the spherical tip on the cone, *R*, the cone opening angle, α, tip-end-to-substrate separation, *d*, and the polarization were then adjusted to monitor the effect on the optical response of the system. Investigations into the effect of altering the cone angle were more inhibited by the limitations of the problem space and Yee cell size. Substantial increases in α cause the tip to cross the problem space boundary at the sides as well as the top, provoking inconsistencies in comparison with systems where the boundary intercepts the tip at the top only. Decreases in α exacerbate problems due to the step edge effect of the Yee cells. The effects of altering the tip-sample separation and radius of the spherical end of the tip are reported in Secs. III and IV, while the result of *s*-polarized excitation is considered in Sec. V.

The problem space was a cube of $120\times120\times120$, 1 -nm^3 Yee cells and time steps five times within the Courant stability limit were used.[32] Implementing fast Fourier transforms on the output yields spectra with a frequency resolution inversely proportional to the total run time of the simulation. Using Yee cells of size greater than $R/10$ causes step edge effects to mask the results. However, since the size of each time step is constrained by the size of the cells used a compromise must be struck between the desired spatial resolution of the problem space and a reasonable frequency resolution for the resulting spectra, in order to keep the computations manageable. The field values for 2^{16} time steps of 0.4×10^{-18} s were calculated, rendering a frequency resolution of 0.16 eV.

In particular, we are interested in the field enhancement directly beneath the tip on the substrate surface for applications in tip-enhanced near-field microscopy and lithography. The ratio, ξ_{tot} of the total electric field, *E*, to the incident electric field, E_0, at the glass-air interface is used as a measure of the enhancement to the local field on the substrate surface

$$\xi_{\text{tot}} = \frac{|E|}{|E_0|}. \tag{2}$$

The enhancement ξ_i to each polarization component was calculated as the ratio of the magnitude of each field component E_i $(i=x,y,z)$ in the presence of the tip to the total field (over all components) in the absence of the tip

$$\xi_i = \frac{|E_i|}{|E_0|}. \tag{3}$$

Unless stated otherwise, the enhancements ξ_x, ξ_y, ξ_z, *and* ξ_{tot} have been determined at the substrate surface directly beneath the tip.

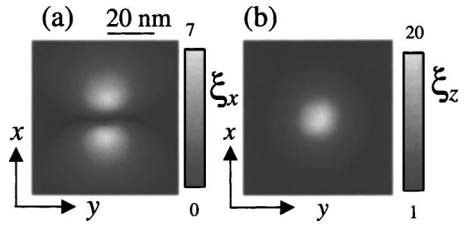

FIG. 3. The *x* (a) and *z* (b) components of the field enhancement distributions on the substrate plane on resonance at 2.46 eV (photon wavelength $\lambda=505$ nm).

The resolution is quantified as the full width at half maximum (FWHM) of the Raman enhancement, *Q*, which is calculated as the fourth power of the field enhancement, as a result of the tip acting as a nanoantenna for both incident and scattered photons. Unless stated otherwise, we assume the Raman scattering to be isotropic, such that,

$$Q = \xi^4 \tag{4}$$

For discussion relevant to molecules for which Raman scattering is only enhanced when the enhancement to the local field is aligned with the axis of Raman-active mode of the molecule, $Q_i=\xi_i^4$.

III. TIP-TO-SURFACE DISTANCE DEPENDENCE

The spectra of the field enhancement, ξ_{tot}, and *z* component, ξ_z, on the substrate surface under *p*-polarized illumination, when the tip is positioned 2 nm above the surface, are shown in Fig. 2(b). The total enhancement spectrum comprises one peak at $\lambda=505$ nm, unequivocally dominated by the contribution of the *z* component. The distribution of the *x* and *z* components to field enhancement on the substrate surface (*xy*) plane is shown at resonance, $\lambda=505$ nm, in Fig. 3. The *z* component of the field is highly concentrated directly beneath the tip on the substrate surface, Fig. 3(b), with a lower yet still appreciable enhancement to the *x* component of the electric field forming lobes at either side while negligible directly beneath the tip [Fig. 3(a)]. Indeed, the in-plane distribution for ξ_x simply reflects the radial nature of the in-plane electric field, as expected from a simple dipole model. Calculations of the charge distribution confirm that the charge is concentrated in a localized surface plasmon at the tip apex. This corresponds to the expected plasmon resonance excited in a system with a high aspect ratio under incident illumination polarized in alignment with the axis of the tip.[23] As the tip is withdrawn, the field enhancement on the surface dwindles rapidly (see Fig. 4) with a decay length of approximately 13 nm, indicating a highly localized plasmon mode. The reader is directed to Ref. 35 for a more extensive investigation into the effect of tip-surface separation on Raman-scattering enhancement.

As well as the decrease in the enhancement, the separation between substrate and the tip also has a potent effect on the resolution. Analyses of field enhancements off resonance at $\lambda=631$ nm, while diminishing the enhancement peaks, do not affect the decay length or the resolution (see Ref. 35),

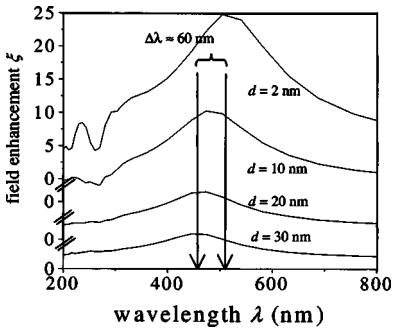

FIG. 4. The enhancement spectra, for *p*-polarized excitation, as a function of wavelength for increasing separations between tip and substrate surface, $d=2$, 10, 20, and 30 nm, as indicated. The blueshift in the resonant wavelength at the substrate surface, directly beneath the tip, $\Delta\lambda_{res}\approx 60$ nm, indicating the effect of the dielectric surroundings on the plasmon field.

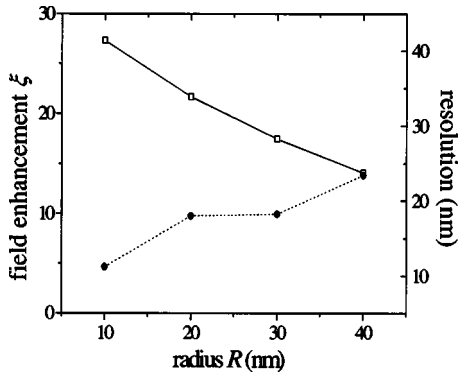

FIG. 5. The effect of tip radius, *R*, on the total enhancement and resolution on the substrate surface beneath the tip (lines are guides to the eye) for *p*-polarized excitation and $d=5$ nm. Increasing *R* diminishes the resolution and the enhancement.

confirming that the system is detuned from resonance but oscillating in the same mode. In addition to the enhancement's diminished impact and dilated profile on the substrate surface in response to increases in the tip-surface separation, there is also a slight blueshift in the position of the resonance peak, $\Delta\lambda=60$ nm from $d=2$ nm and $d=30$ nm, indicated in the spectrum in Fig. 4. This shift, which is equivalent to only twice the frequency resolution for these calculations, has been confirmed with higher-resolution calculations for which the total time and hence frequency resolution were doubled using a Yee cell size of 2 nm. The resonance in the spectrum taken at the tip apex rather than on the substrate surface does not shift with increases in *d* and the wavelength at which the incident pulse peaked was not found to affect the position of the resonance peak in the field enhancement. Resonance shifts have been noted as a consequence of the sensitivity of plasmon resonances to the dielectric environment, attributed to the excitation of higher-order surface-plasmon resonances.[29,30] Moreover, in line with the blueshift which we observe, Ref. 29 predicts a blueshift with increasing *d* for small silver ellipsoids. This blueshift is also identified in Ref. 30 for small spherical nanoparticles and, in line with the results of our own calculation of a metal tip, these authors calculated a blueshift for larger nanoparticles, which is probably more representative of a real infinitely long tip.

IV. TIP RADIUS DEPENDENCE

Figure 5 shows the effect on the total field enhancement on the surface directly beneath the tip and the resolution, quantified as the FWHM of the Raman enhancement, as the radius *R* is altered between 10 and 40 nm. Both the field enhancement and the Raman resolution have deteriorated, as may be expected, as the radius of curvature is increased. In addition, the decay length of the field enhancement increases from 13 to 18 nm as the tip radius is increased from $R=20$ to 40 nm. However, we note that at resonance a spatial Raman resolution far sharper than the tip radius can be achieved. The resonance spectra (Fig. 6) for the *x* and *z* components of the electric-field enhancement on the substrate surface beneath the 40-nm radius tip seem to indicate that the enhancement dominated by the *z* component at $\lambda=474$ nm is succumbing to a competing higher-energy mode which forms a shoulder in both the *x* and *z* components at $\lambda=303$ nm. The field distributions in the substrate plane for excitation resonant with these two modes are shown in Fig. 7. The asymmetry about the (*yz*) plane is mirrored in the charge distribution and may be a numerical artifact. However, the differences in the distribution of the components to the field enhancement are sufficiently substantial to indicate that the mode oscillating at $\lambda=303$ nm is distinct from the mode oscillating at $\lambda=505$ nm.

V. EXCITATION POLARIZATION DEPENDENCE

As may be supposed, the *z* component dominates the enhancement when the incident illumination is *p*-polarized along the tip axis.[36–38] Indeed, illumination configurations have been identified in which the *z* component dominates the incident field at the center of a focused spot.[39] While the most impressive field enhancements on the surface beneath the tip at $d=2$ nm occur under *p*-polarized illumination, it is sometimes desirable to have the field components parallel to the surface preferentially enhanced.[11] With this in mind, we have also calculated the field values for a tip-substrate system in which the incident pulse is polarized perpendicular to the plane of incidence. The enhancements in the substrate

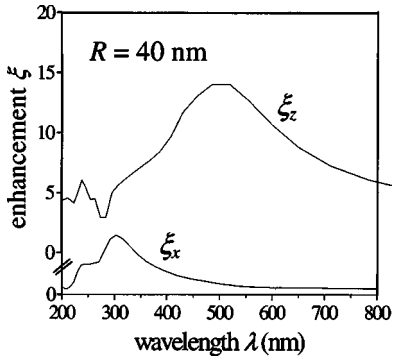

FIG. 6. Resonance spectra for ξ_x, the *x* component, and ξ_z, the *z* components of the field enhancement at the center of the substrate surface ($R=40$ nm and $d=5$ nm). The increase in the *x* component at $\lambda=303$ nm suggests that the overall enhancement at the larger resonance at 505 nm may be diminished due to competition between modes.

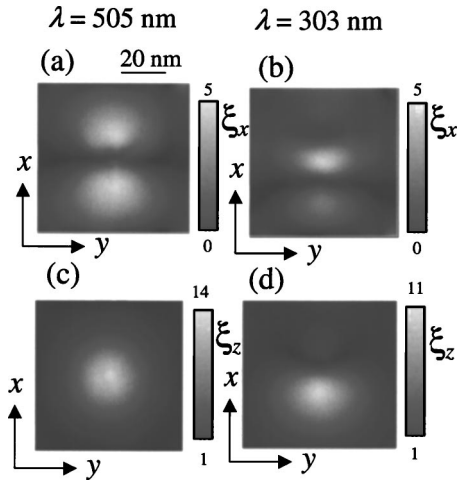

FIG. 7. Field enhancement distributions for (a), (b) ξ_x and (c), (d) ξ_z on the substrate surface at (a), (c) $\lambda = 505$ nm and (b), (d) $\lambda = 303$ nm, corresponding to the two plasmon modes identified in the resonance enhancement spectra in Fig. 6.

plane and perpendicular to the substrate plane were subsequently compared under *p*-polarized and *s*-polarized illuminations, respectively.

Figures 8(a) and 8(b) show the field distributions in the substrate plane for the different components at resonance, $\lambda = 292$ nm. At no point in the plane does the field enhancement reach the magnitude achieved under *p*-polarized illumination. Although to either side the *z* component begins to take prevalence, the *y* component dominates directly beneath the tip on the substrate surface. Under *s*-polarized illumination the charge is concentrated at either side of the tip in contrast with the case of *p*-polarized illumination for which the charge is concentrated at the tip apex.

Figure 9 shows the enhancement spectra for the *y* and *z* components of the electric field at a point on the substrate surface displaced by $\Delta y = 11$ nm from the point directly beneath the tip [indicated by the cross in Fig. 8(b)]. The photon wavelength, $\lambda = 292$ nm, corresponding to a photon energy of 4.26 eV, at which the system is at resonance under *s*-polarized illumination, is beyond the range for which our Drude model provides a reasonable approximation of silver; so although the model still describes a metal tip over a glass surface, that metal may no longer be considered to simulate silver. However, from the field distributions in Fig. 8 and the peaks dominating the enhancement resonance spectra in Fig. 9, it is clear that a plasmon resonance maximizing in-plane components of the field enhancement is excited under *s*-polarized illumination.

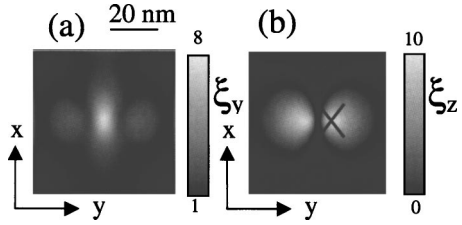

FIG. 8. (a) *y* and (b) *z* components of the field enhancements on the substrate surface for *s*-polarized excitation. The cross in (b) marks the point on the substrate where the *z*-field enhancement reaches a maximum.

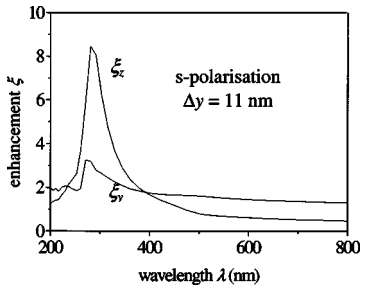

FIG. 9. Comparison of *y* and *z* components to the field enhancement, 11 nm to the side of the center of the substrate as indicated by the cross in (b). The *y* field has fallen to less than half its value directly beneath the tip at this point.

In-plane enhancements of comparable magnitudes also occur under *p*-polarized illumination in the lobes, as seen in Fig. 3(a). However, the distribution of the in-plane enhancement offered under *s*-polarized illumination is more accommodating for applications such as Raman microscopy. Being centralized under the tip, in the latter case, there will be less problems associated with double images than may arise from enhancements in two distinct lobes, although there are subsidiary maxima in the in-plane enhancement to either side [ξ_y in Fig. 8(a)], which will serve to reduce resolution. The emphasis on enhancements in the substrate plane as opposed to perpendicular to the substrate is eminently relevant to studies for which coupling between field enhancements and molecules orientated parallel to the substrate surface is desired, such as in the case of tip-enhanced Raman scattering from single-walled carbon nanotubes.[11]

Figure 10 shows a comparison between the stronger of the in-plane components of the Raman enhancement, i.e., the *x* and *y* components for *p*- and *s*-polarized illuminations, respectively. The spectra correspond to the point on the substrate surface directly beneath the tip, and illustrate that the Raman enhancement to an in-plane component is greater under *s*-polarized illumination. It should also be noted that while here we have considered the system illumined under the same configuration with different polarizations for consistency, calculations have been made for which the incident angle was altered to 0° instead and the results were similar to the field distributions and trends of using *s*-polarized illumination.

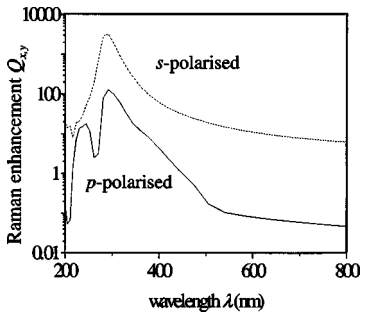

FIG. 10. Comparison of the Raman field enhancements in the substrate plane for *s*-polarized (dashed) and *p*-polarized (solid) illuminations. The tip-to-surface separation is 5 nm and the greater of the in-plane field components is shown, i.e., *x* field for *p* polarized and *y* field for *s* polarized.

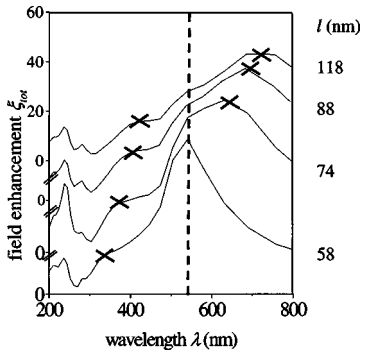

FIG. 11. The effect, on the resonant fields at the substrate surface, of the length of tip, *l*, within the problem space: $l=58$, 74, 88, and 118 nm. Resonances at $\lambda=300-450$ nm (marked with X's) and $\lambda=600-750$-nm shift to longer wavelengths as the tip length increases, but the tip-localized plasmon resonance at $\lambda=541$ nm (marked by the dashed vertical) stays constant, although it appears as a shoulder as other resonances dominate.

VI. AN ASSESSMENT OF THE MODEL: THE EFFECT OF SIMULATED TIP LENGTH

In order to evaluate the proficiency of our approximation to an extended tip, the effect of altering the length of tip within the problem space was investigated. Figure 11 shows a series of spectra as the length of tip within the problem space was increased. Certain trends in the structure can be distinguished, such as the increasingly prominent shoulders around $\lambda=400$ nm and $\lambda=690$ nm which almost swallow the resonance associated with the localized plasmon mode (this appears at $\lambda=541$ nm, a difference from $\lambda=505$ nm, as indicated in Fig. 4, equivalent to the frequency resolution of the fast Fourier transform when using the larger Yee cells to explore larger problem spaces). The alterations to the spectra as tip length is increased can be understood by considering the excitation of extended rather than localized surface-plasmon modes excited in the system. As the length of tip within the problem space was increased from 60 to 120 nm, the appearance of extended surface plasmons became apparent, as indicated by the crosses in the spectra in Fig. 11.

In fact, an extended surface plasmon appears to be excited when only 58 nm of the tip is within the problem space as in the standard configuration described above, but at a shorter wavelength (higher energy) it is weaker. Increasing the size of the tip causes redshifts in these extended surface-plasmon modes in accordance to the behavior of the Fröhlich frequency of spherical particles of finite size,[37] but the resonance associated with the localized plasmon at $\lambda=541$ nm remains, albeit weakened by the competing surface-plasmon mode. As this surface-plasmon resonance is highly localized and excited whatever the tip length, we can conclude that our system can be considered to approximate an extended tip in the absence of artifact extended surface modes corrupting the enhancement spectra. For a true infinitely extended tip we may expect to recover a response from just the localized mode and with respect to these modes we consider our system to achieve an adequate approximation.

The failure of boundary conditions where the tip meets the boundary is likely to arise from deficiencies in the use of a buffer layer with a frequency-independent dielectric response between the Drude silver and the boundary. The dielectric constant of the buffer is matched to that of the tip at 3 eV ($\lambda=414$ nm), but at lower energies the dielectric response of the tip diverges increasingly from the constant value of the buffer, apparent from Fig. 2(a). This approximation to an extended tip has evident limitations. However, it is fortunate that in the original regime using a 58-nm tip, the surface modes associated with the finite size of the tip do not dominate the system and so do not warp what may be considered the optical response of an extended tip system.

VII. CONCLUSIONS

Numerical calculations have demonstrated a steep dependence on tip-to-surface separation of the electric-field enhancement beneath a silver tip. The effect of detuning from the resonance wavelength, with respect to enhancement and resolution achievable in tip-enhanced Raman SNOM, emphasizes the prominence of the role localized plasmons play in near-field enhancements. Shifts in the resonant wavelength as the separation between the tip and the surface is altered have demonstrated the substrate's effects on the propagation of the scattered fields. Increasing the radius of curvature of the end of the probe was found to diminish the overall enhancement and resolution and to allow the excitation of higher-order plasmon modes. The enhancements on the surface from *s* polarization are lower than those using *p*-polarized illumination, but the enhancement component along the surface directly beneath the tip is maximized in *s* polarization. This is greater than the stronger of the in-plane enhancements proffered by the system under *p* polarization, although it should be emphasized that this is only the case directly beneath the tip. The limitations of the approximation to an extended tip system have also been defined and are not believed to affect the conclusions drawn from the current study.

ACKNOWLEDGMENTS

We would like to thank Robert Milner for his initial development of the code. We are grateful to the EPSRC for their support.

[1] C. Girard, C. Joachim, and S. Gauthier, Rep. Prog. Phys. **63**, 893 (2000).
[2] K. Kneipp, H. Kneipp, I. Itzkan, R. R. Dasari, and M. S. Feld, J. Phys.: Condens. Matter **14**, 597 (2002).
[3] D. Richards, Philos. Trans. R. Soc. London, Ser. A **361**, 2843 (2003).
[4] S. Grésillon, L. Aigouy, A. C. Boccara *et al.*, Phys. Rev. Lett. **82**, 4520 (1999).
[5] F. H'dhili, R. Bachelot, G. Lerondel, D. Barchiesi, and P. Royer, Appl. Phys. Lett. **79**, 4019 (2001).
[6] S. Klein, T. Witting, K. Dickmann, P. Geshev, and M. Hietschold, Single Mol. **3**, 281 (2002).
[7] R. G. Milner and D. Richards, J. Microsc. **202**, 66 (2001).
[8] D. Richards, R. G. Milner, F. Huang, and F. Festy, J. Raman Spectrosc. **34**, 663 (2003).
[9] J. T. Krug II, E. J. Sanchez, and X. S. Xie, J. Chem. Phys. **24**, 10895 (2002).
[10] X.-Q. Wang, S.-F. Wu, G.-S. Jian, and S. Pan, Phys. Lett. A **319**, 514 (2003).
[11] A. Hartschuh, E. J. Sanchez, X. S. Xie, and L. Novotny, Phys. Rev. Lett. **90**, 095503 (2003).
[12] R. Fikri, T. Grosges, and D. Barchiesi, Opt. Commun. **232**, 15 (2003).
[13] L. Novotny, R. X. Bian, and X. S. Xie, Phys. Rev. Lett. **79**, 645 (1997).
[14] N. Calander and M. Willander, Phys. Rev. Lett. **89**, 143603 (2002).
[15] P. C. Chaumet, A. Rahmani, and M. Nieto-Vesperinas, Phys. Rev. B **66**,

195405 (2002).
[16]C. Girard, O. J. F. Martin, and A. Dereux, Phys. Rev. Lett. **75**, 3098 (1995).
[17]J.-M. Segura, G. Zumofen, A. Renn, B. Hecht, and U. P. Wild, Chem. Phys. Lett. **340**, 77 (2001).
[18]W. Trabesinger, A. Kramer, M. Kreiter, B. Hecht, and U. P. Wild, Appl. Phys. Lett. **81**, 2118 (2002).
[19]A. Kramer, W. Trabesinger, B. Hecht, and U. P. Wild, Appl. Phys. Lett. **80**, 1652 (2002).
[20]K. Kneipp, Y. Wang, H. Kneipp, L. T. Perelman, I. Itzkan, R. R. Dasari, and M. S. Feld, Phys. Rev. Lett. **78**, 1667 (1997).
[21]N. Felidj, J. Auberd, G. Lévi, J. R. Krenn, A. Hohenau, G. Schider, A. Leitner, and F. R. Aussenegg, Appl. Phys. Lett. **82**, 3095 (2003).
[22]S. Hudlet, S. Aubert, A. Bruyant *et al.*, Opt. Commun. **230**, 245 (2004).
[23]J. P. Kottmann, O. J. F. Martin, D. R. Smith, and S. Shultz, Opt. Express **6**, 213 (2000).
[24]T. Kalkbrenner, M. Ramsten, J. Mlynek, and V. Sandoghdar, J. Microsc. **202**, 72 (2001).
[25]R. A. Molina, D. Weinmann, and R. A. Jalabert, Phys. Rev. B **65**, 155427 (2002).
[26]T. R. Jensen, M. D. Malinsky, C. L. Haynes, and R. P. Van Duyne, J. Phys. Chem. **104**, 10549 (2000).
[27]S. J. Oldenburg, S. L. Westcott, R. D. Averitt, and N. J. Halas, J. Chem. Phys. **111**, 4729 (1999).
[28]K. Chatterjee, S. Banerjee, and D. Chakravorty, Phys. Rev. B **66**, 085421 (2002).
[29]J. Renger, S. Grafström, L. M. Eng, and V. Deckert, J. Opt. Soc. Am. A **21**, 1362 (2004).
[30]J. A. Porto, P. Johansson, S. P. Apell, and T. López-Ríos, Phys. Rev. B **67**, 085409 (2003).
[31]F. I. Baida, D. Van Labeke, and Y. Pagani, Opt. Commun. **225**, 241 (2003).
[32]K. S. Kunz and R. J. Luebbers, *The Finite Difference Time Domain Method for Electromagnetics* (CRC, Boca Raton FL, 1993).
[33]P. B. Johnson and R. W. Christy, Phys. Rev. B **6**, 4370 (1972).
[34]Taflove, *Computational Electrodynamics The Finite Difference Time-Domain Method* (Artech House, Boston, 1995).
[35]F. Festy, A. Demming, and D. Richards, Ultramicroscopy **100**, 437 (2004).
[36]A. Bouhelier, J. Renger, M. R. Beversluis, and L. Novotny, J. Microsc. **210**, 220 (2003).
[37]W. X. Sun and Z. X. Shen, Ultramicroscopy **94**, 237 (2003).
[38]F. Bohren and D. R. Huffman, *Absorption and Scattering of Light by Small Particles* (Wiley, New York, 1998).
[39]L. Novotny, E. J. Sánchez, and X. S. Xie, Ultramicroscopy **71**, 21 (1998).